C. R. Chimie 18 (2015) 379–384

Contents lists available at ScienceDirect

Comptes Rendus Chimie

www.sciencedirect.com

Full paper/Mémoire

Fabrication of hollow spheres of metal oxide using fructose-derived carbonaceous spheres as sacrificial templates

Haitham Mohammad Abdelaal [a,b,*], Bernd Harbrecht [b]

[a] Ceramics Department, National Research Centre, PO 12622, Dokki, Cairo, Egypt
[b] Department of Chemistry and Centre of Materials Science Philipps University, 35032 Marburg, Germany

ARTICLE INFO

Article history:
Received 16 March 2014
Accepted after revision 18 August 2014
Available online 4 March 2015

Keywords:
Materials science
Electron microscopy
Mesoporous materials
Carbohydrates
Scanning probe microscopy

ABSTRACT

In this report, fructose-derived carbonaceous spheres were utilized as sacrificial templates for the fabrication of metal oxide hollow spheres (MOHSs) by a facile hydrothermal approach. Hollow spheres of a series of crystalline metal oxides (α-Fe_2O_3, Cr_2O_3, Co_3O_4, NiO, and ZnO) have been fabricated, utilizing the metal chloride as the oxide precursors. Heating of an aqueous solution of the metal chloride and fructose to moderate temperature in an autoclave affords a spherical composite consisting of a metal precursor shell sheathing a carbonaceous core. Subsequent removal of the interior carbonaceous cores by thermal treatment through oxidation in air produces free-standing crystalline oxides hollow spheres. The MOHSs were characterized by means of SEM, TEM, XRD, IR spectroscopy, energy dispersive X-ray (EDX) and sorption measurements. The results show convincingly that using fructose as a sacrificial template after application of a hydrothermal synthesis route could be a favourable sacrificial template for the fabrication of various MOHSs.

1. Introduction

Metal oxide hollow particles have shown to be promising as inorganic containers and vehicles in various applications, such as catalysis, Li-ion batteries, water treatment, photonic devices, chemical sensors, prosthetic materials and controlled release applications [1–6]. To date, inorganic hollow particles have been fabricated by using various novel mechanisms [7–11].

Indeed, in the last decades, the research activity for the fabrication of oxide hollow micro- and nanoparticles has increased largely due to their unique and enhanced properties, such as low density, hollow cores and large specific surface area combined with the various functions of oxides. For instance, it has been shown that hollow particles can be readily fabricated by using the nanoscale Kirkendall effect [12]. In addition, a well-known physical phenomenon of crystal growth – Ostwald ripening – has been applied for the fabrication of hollow materials [13]. As another synthesis mechanism, Messing et al. reported the formation of hollow particles with different morphologies using a variety of spray pyrolysis techniques [14]. Caruso et al. introduced the colloidal templating synthesis of hollow spheres for the first time in 1998 [15].

Among many synthesis mechanisms, sacrificial templating methods are considered as the most often used strategies. They are relying on the formation of core-shell composites and subsequent removal of the core by

* Corresponding author.
E-mail address: hmaa_77@yahoo.com (H.M. Abdelaal).

http://dx.doi.org/10.1016/j.crci.2014.08.004
1631-0748/

chemical or thermal means [16]. These methods have been developed considerably and the templates used are divided into:

- hard templates, including colloidal templates such as polymer [17] and silica spheres [18];
- soft templates, including surfactant vesicles and micro-emulsion droplets [16,19].

Xie et al. reported synthesized rutile-phase TiO_2 hierarchical hollow spheres using gas bubbles as a soft template [20]. Chen et al. reported the use of organic templates for the synthesis of silica hollow particles through sacrificial templating approach via the removal of the template by thermal treatment [21].

Latterly, carbohydrate-derived carbonaceous spheres, which are formed through the hydrothermal carbonization of aqueous solutions of saccharides, have been used successfully as sacrificial templates for the synthesis of hollow inorganic particles [22–24]. These sacrificial cores possess surface functionalities that facilitate the adsorption of the desired materials precursors onto their reactive surfaces, as shown by Li et al. [23] and Thomas et al. [24] for different hollow materials.

Among the potential saccharides that can be used as sacrificial templates for the synthesis of inorganic hollow structures, fructose is one of the most promising materials, as it is by far one of the most inexpensive and widely available saccharides. Although many researchers reported using carbohydrates as sacrificial templates for the synthesis of inorganic hollow particles [22–26], to the best of our knowledge, no one has employed fructose as the sacrificial template for the fabrication of hollow spheres by means of hydrothermal carbonization.

In the present contribution, we report a facile hydrothermal approach for the fabrication of series of oxide hollow spheres (α-Fe_2O_3, Cr_2O_3, Co_3O_4, NiO and ZnO) using fructose as the sacrificial template. The synthesis method shows some advantages, which likely make it attractive for the fabrication of other oxide hollow spheres, include:

- the use of inexpensive fructose as sacrificial template;
- fructose-derived carbonaceous spheres, formed by the hydrothermal hydrolysis of fructose, inherit surface O-functionalities, such as –C=O and–OH groups [27] – therefore, there is no need for prior surface modifications;
- only the template and the metal precursor are used for the fabrication of the hollow oxide spheres, thus, there is no need for any chemical additives;
- the fabrication method is a simple strategy that can be readily analyzed and manipulated in comparison to complex multi-step strategies with many procedures and a variety of chemical additives.

2. Materials and methods

2.1. Materials

Iron(III) chloride hexahydrate ($FeCl_3{\cdot}6H_2O$), chromium(III) chloride hexahydrate ($CrCl_3{\cdot}6H_2O$), cobalt(II) chloride hexahydrate ($CoCl_2{\cdot}6H_2O$), zinc(II) chloride ($ZnCl_2$) and nickel(II) chloride ($NiCl_2$) were obtained from Merck (Darmstadt, Germany). Commercial fructose ($C_6H_{12}O_6$) was bought from dm-drogerie markt, Germany. All mentioned chemicals were analytical grade and employed without further purification. Distilled water (conductivity $\sim 1.7\ \mu s{\cdot}cm^{-1}$) was used.

2.2. Fabrication of the metal oxide hollow spheres (MOHSs)

The major process step applied in the present work starts with heating the metal chloride with fructose in a closed system resulting in in situ formation of hybrid particles, due to the incorporation of the metal ions on the surface layers of the fructose-derived carbonaceous spheres. Finally, calcination of the hybrid spheres leads to the formation of the MOHSs.

In a typical synthesis experiment, 2252 mg (12.5 mmol) of fructose were dissolved in 20 mL of distilled water. The water-soluble metal chloride during the hydrothermal carbonization was added to satisfy the fructose/metal chloride molar ratio 20:1. The mixture was heated in a 100-mL Teflon-lined stainless steel autoclave at 135 °C for 6 h. The products were filtered off, washed three times with distilled water, and finally dried in a vacuum oven at 60 °C for 5 h. Thereafter, the metal oxide–carbon composites were calcined in the air at 500 °C (with a heating rate of 2 °C min^{-1}) for 5 h to remove the carbonaceous core, thus leading to the metal oxide hollow particles.

2.3. Characterization

The products were characterized by various techniques. Infrared (IR) spectra were obtained using IFS 88 from Bruker. XRD patterns were obtained by X-ray powder diffraction (X'Pert MPD, Pananalytical, Cu Kα radiation) operating in Bragg–Brentano geometry [28]. The diffractometer was equipped with a graphite monochromator at the detector side. The sample holder was a single-crystal silicon plate. The energy dispersive X-ray (EDX) analysis was performed using Thermo Noran Voyager EDX system attached to a CamScan series 4 Scanning Electron Microscope from Cambridge Scanning Company Ltd.

The surface area was studied by nitrogen-sorption measurements, which were performed with the use of a Micromeritics ASAP 2020 gas sorptometer. The samples were degassed in vacuo at a pressure of 0.4 Pa for at least 3 h at 200 °C. The measurements were then carried out at 77 K over a wide range of relative pressures from 0.01 to 0.995. Specific surface areas were calculated by assuming Brunauer–Emmet–Teller (BET) conditions.

The morphology was visualized using a JEOL JSM-7500F field emission scanning electron microscope at an accelerating voltage of 5 kV. Hereford, samples were ground to a powder and then mounted on an aluminum stub with a conductive carbon tape and, for electrically nonconductive samples, a thin layer of platinum coating was applied before SEM analysis. Transmission electron microscopy (TEM) was conducted on a JEOL model JEM-3010 electron microscope operating at 300 kV. The samples were ground into powder and mounted by drop

drying of a chloroform suspension onto TEM cupper grids before TEM analysis.

3. Results and discussion

Fructose has been successfully utilized as the sacrificial template for the fabrication of inorganic oxide hollow spheres through sacrificial templating procedures. Hollow spheres of α-Fe_2O_3, Cr_2O_3, Co_3O_4, NiO and ZnO with wall composed of the oxide nanoparticles have been comfortably produced through this method.

Fig. 1 illustrates schematically the mechanism proposed for the formation of porous metal oxide hollow spheres (MOHSs). The formation of MOHSs probably involves four stages:

- autoclaving of the reactants (fructose + metal chloride) at moderate temperature involves the dehydration and subsequent carbonization of fructose resulting in carbonaceous spheres (CSs). The surface layers of these CSs are hydrophilic and rich in oxygen functionalities (e.g. –OH, C=O) due to non- or partially-dehydrated fructose [27,29,30];
- the metal ions dispersed in the solution mixture can anchor onto the surface of the CSs and bind with the functional groups in the surface layers by taking advantage of co-ordination or electrostatic interactions. This leads to the in situ formation of core@shell composite consisting of fructose-derived carbonaceous spheres with the metal ions bound to the oxygen functionalities in the outer shell;
- eventually, the carbonaceous cores are removed by pyrolytic treatment in the air. Hence, the surface layer, incorporating the cationic metal ions, is densified and cross-linked to form the free-standing hollow spheres replicas of the CSs though about 40 to 60% smaller than the size of the original composite particles. The significant shrinkage in size during the thermal treatment indicates that the metal cations adsorbed on the surface of the cores have been transformed into dense networks of nanocrystalline metal oxides grains that compose the shells of the hollow spheres [23,24];
- frequently, the resulting MOHSs show a ball in ball (bnb) hollow structure that is formed without any extra step. To date, the mechanism of formation of the bnb structure is less well-known and an open question to material scientists. Yet, it was postulated that some nano-islands of metal oxide nanoparticles in the shell may migrate to or be stuck on the surface of the shrinking CSs cores in the course of the calcination process. Upon further heating at elevated temperature, these nano-islands finally aggregate into a small hollow ball in the interior when the CSs cores are completely burnt off [30–32].

The XRD patterns in Fig. 2, recorded from the samples after calcination at 500 °C for 5 h, show that the MOHSs consist of the well-crystalline single-phase metal oxide as shown by Rietveld refinement of the XRD patterns (Fig. S1).

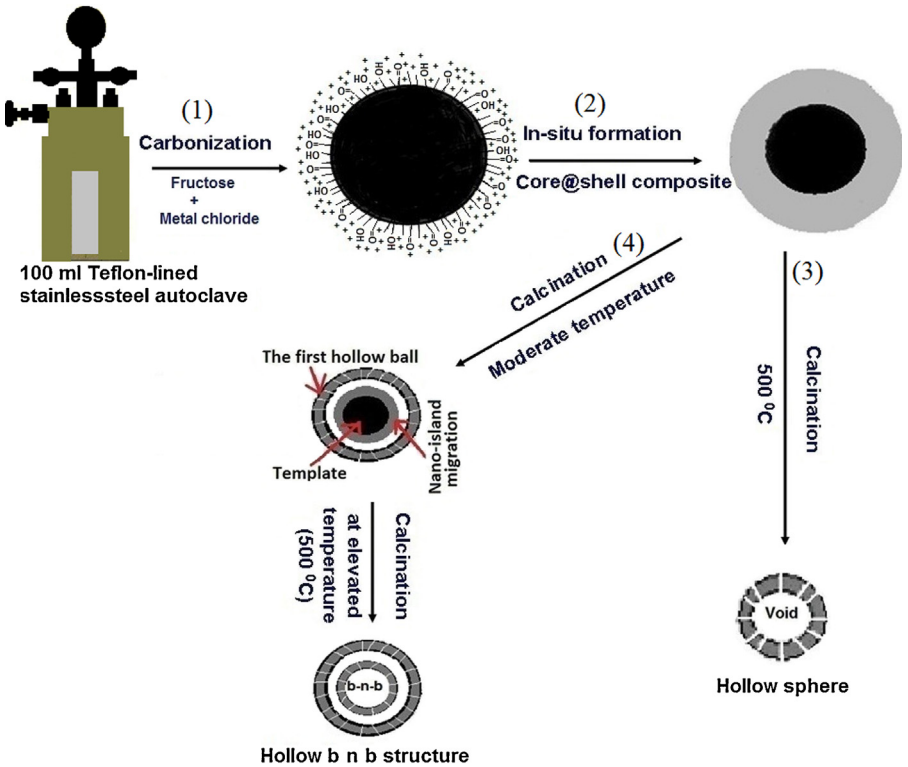

Fig. 1. (Color online.) Schematic diagram of the fabrication of porous metal oxide hollow spheres by hydrothermal method.

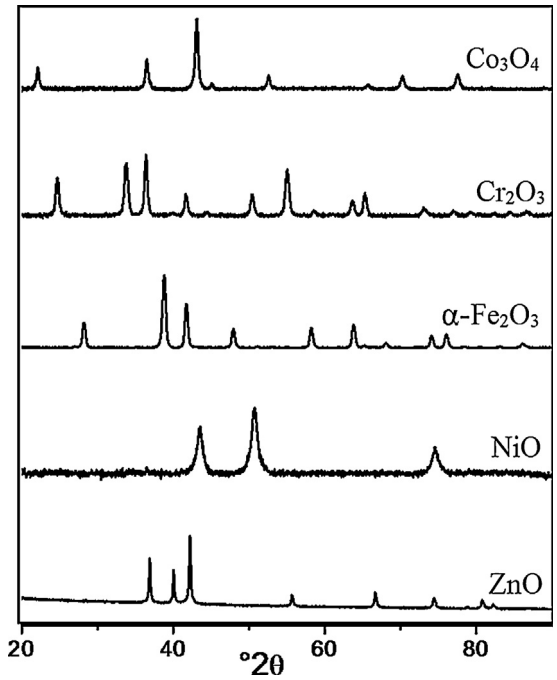

Fig. 2. XRD patterns of the as-obtained oxide hollow spheres.

The average crystallite size was calculated by applying Scherrer's equation (which assumes the small crystallite size to be the cause of line broadening) using the full-width at half maximum (FWHM) of the most intense peaks [33]. The average crystallite sizes were determined to be 19, 17, 21, 10, 35 nm for α-Fe_2O_3, Cr_2O_3, Co_3O_4, NiO, and ZnO, respectively. No crystalline peaks were observed before calcination (Fig. S1), revealing that the metal ions are evenly adsorbed onto the hydrophilic surface of the CSs or dispersed in the surface as amorphous cluster after the hydrothermal treatment.

The comparison between IR spectra before and after calcination demonstrates the removal of the carbonaceous template material and the formation of the MOHSs, as shown in Fig. 3 for Cr_2O_3 hollow spheres. The IR spectrum before calcination shows a broad peak between 3000 cm^{-1} and 3500 cm^{-1}, which is likely to be the stretching vibration of O–H and the peak at 2900 cm^{-1} is belonging to the stretching vibration of the C–H bond. The vibrations at 1700 cm^{-1} and 1611 cm^{-1} can be assigned to C=O and C=C, respectively. The C=C double bonds indicate that dehydration has taken place during the hydrothermal carbonization of fructose [34,35]. After calcination, the carbonaceous templates and most peaks related to the functionalities, like carboxylic or aromatic groups, are gone.

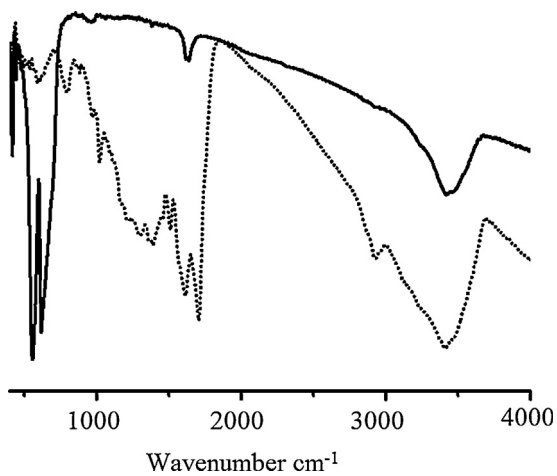

Fig. 3. IR spectra of the as-obtained Cr_2O_3 hollow spheres, before and after calcination at 500 °C for 5 h ····· before calcination; ⁻⁻⁻ after calcination.

In Fig. 3, which represents Cr_2O_3 hollow spheres, a peak at 3400 cm^{-1} is likely to be the O–H stretching vibration of surface Cr–OH groups and the absorption at 1600 cm^{-1} is due to the stretching and bending modes of surface-adsorbed/trapped (hydrogen-bonded) water molecules. The peaks at 560 and 621 cm^{-1} are typical peaks for Cr_2O_3, which were ascribed to the stretching vibration of Cr–O bonds [36].

The inset in Fig. 4a shows the TEM micrograph of the core@shell composite before calcination of α-Fe_2O_3. We can notice that a contrast appears in the image between the shell material and the core material. This provides support for the assumption of the spatial separation of the metal ions rich shell and the carbonaceous cores. After calcination at 500 °C for 5 h, the carbonaceous materials are completely removed, leaving free-standing hollow α-Fe_2O_3 spheres, as seen in Fig. 4b.

SEM micrographs in Fig. 5 illustrate the hollow spheres of Cr_2O_3, Co_3O_4, NiO, and ZnO after calcination. SEM micrographs of the products in Fig. 5 evidence the formation of the spherical hollow oxides particles. A careful observation of the surface of the hollow spheres shows that the walls of the MOHSs are composed of many small nanoparticles of the metal oxide. From the broken shell, marked with an arrow, we can see the hollow porous nature of the MOHSs. These observations indicate that after calcination, the spheres remained intact and preserved the three-dimensional spherical shape of particles after removing the carbonaceous core material (Figs. 4 and 5 and Figs. S2, S3 for the samples before calcination). This denotes that the fructose-derived CSs essentially are the shape-directing agent.

The TEM micrographs (Figs. 4 and 5) are further confirmation of the hollow interior clearly. We can observe a contrast between the dark shell and the pale core. In addition, a reduction in size by about 40–60% takes place after calcination, as seen from the particle size distribution of the samples before and after calcination (Fig. S4). Obviously, the metal ions, incorporated in the surface layer of the template, density and cross-link through the thermal treatment to form the metal oxide hollow spheres replicas of the template with significantly reduced size.

EDX data of Cr_2O_3 hollow spheres in Table 1 (see also Fig. S5) reveal that it is composed only of Cr and O after calcination at 500 °C for 5 h and Cr, O and C before calcination, without any other impure elements, as listed in Table 1.

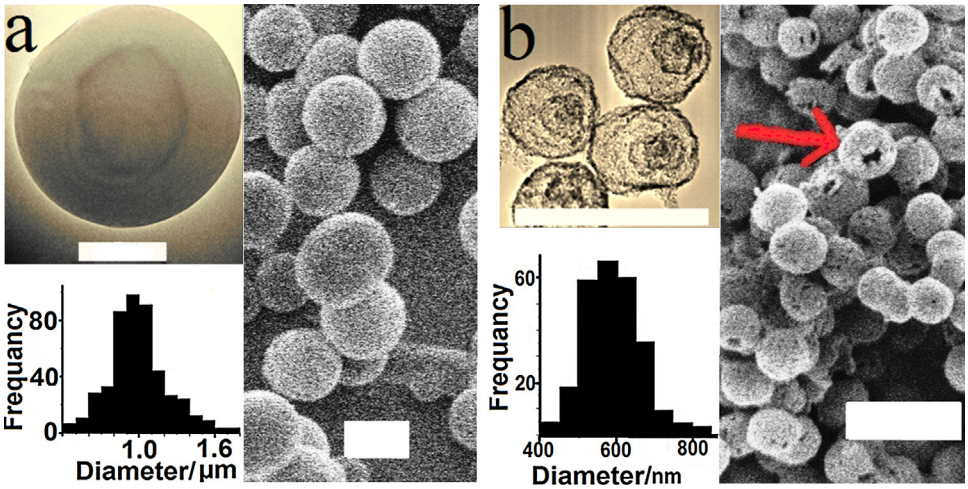

Fig. 4. (Color online.) SEM micrographs of hollow α-Fe_2O_3, (a) before calcination, (b) after calcination at 500 °C for 5 h; the insets are the TEM micrographs and the particle size distribution of the corresponding samples; the scale bare is 1 μm; the arrow refers to a broken shell.

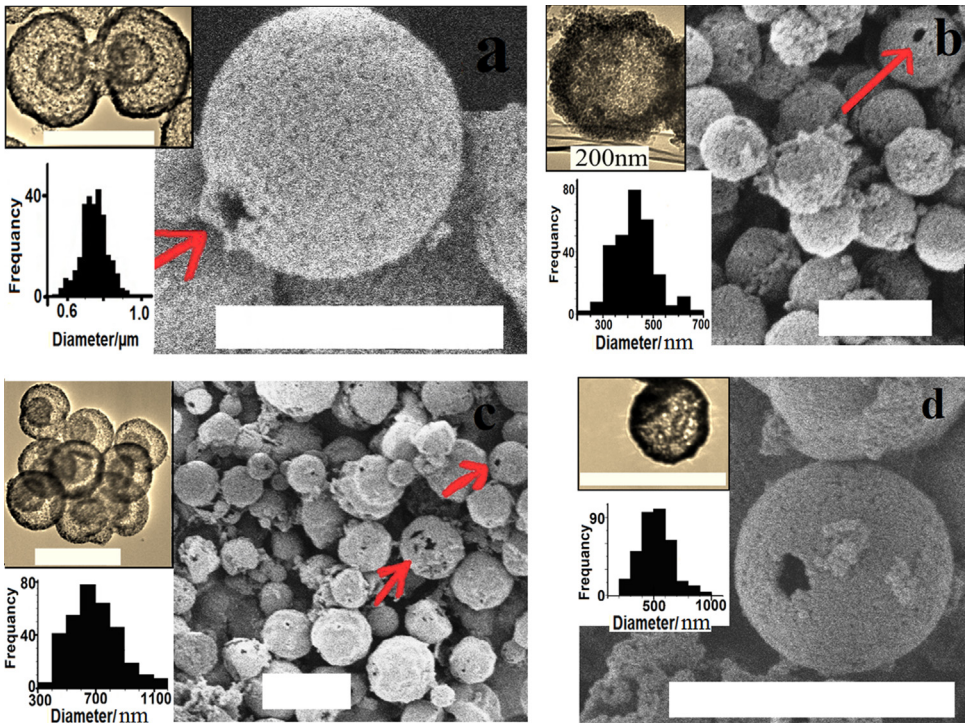

Fig. 5. (Color online.) SEM micrographs of the as-obtained hollow oxides after calcination at 500 °C for 5 h: (a) Cr_2O_3, (b) Co_3O_4, (c), NiO (d) ZnO hollow spheres; the insets are the TEM micrographs and the particle size distribution of the corresponding samples; the scale bare is 1 μm, except the TEM inset micrograph in b; the arrow refers to a broken shell.

The nitrogen adsorption/desorption isotherms were measured to study the porosity and specific surface area of the as-synthesized MOHSs (Fig. S6). These isotherms are characteristic of mesoporous materials according to the International Union of Pure and Applied Chemistry (IUPAC) [37]. Hysteresis loops can be observed in the curves of all samples, evidencing the existence of the mesoporous structure. The surface areas of the as-synthesized MOHSs are 51, 55, 47, 48, 60 $m^2 \cdot g^{-1}$ for α-Fe_2O_3, Cr_2O_3, Co_3O_4, NiO, and ZnO hollow spheres, respectively. The specific surface areas of these MOHSs are assigned to the combination of the surface area of the outer surface, the inner surface and the primary pores, which altogether form the surface area of the particles.

Table 1
Element composition in wt%.

Sample	Cr	O	C
Before calcination	21	45	34
After calcination	68	32	–

4. Conclusion

In conclusion, fructose has been successfully utilized as a sacrificed template for the synthesis of some inorganic oxide hollow spheres using a facile hydrothermal route. After heating of an aqueous solution of the metal chloride and fructose to moderate temperature in a closed system, spherical core-shell composites consisting of the metal precursor shell sheathing a carbonaceous core are formed. After thermal treatment of the core-shell composites, the MOHSs are produced. Though the calcination of the composites gives rise to a drastic shrinkage in size, the spherical shape is preserved. The success of utilizing the fructose-derived CSs as sacrificial templates is likely because of their surface functional layers. Thus, it makes an additional modification of the surface of the shape-controlling carbonaceous template unnecessary and provides the homogeneity of the shell.

A series of porous metal oxides hollow spheres (α-Fe_2O_3, Cr_2O_3, Co_3O_4, NiO and ZnO) have been successfully obtained in this way. As a result, we believe that using fructose as a sacrificial template after application of a hydrothermal synthesis route could be a favourable sacrificial template for the fabrication of other MOHSs.

The metal oxide spheres with hollow interior cores, large specific surface area and mesoporous walls combined with the diverse functions of the oxide may be found with potential applications in various fields such as catalysis, water treatment, photonic devices, chemical sensors and controlled release applications, for example.

Appendix A. Supplementary data

Supplementary data associated with this article can be found, in the online version, at http://dx.doi.org/10.1016/j.crci.2014.08.004.

References

[1] H.P. Liang, H.M. Zhang, J.S. Hu, Y.G. Guo, L.J. Wan, C.L. Bai, Angew. Chem. 116 (2004) 1566.
[2] (a) J. Liu, H. Xia, D. Xue, L. Lu, J. Am. Chem. Soc. 131 (2009) 12086;
(b) J. Liu, Y. Wan, C. Liu, W. Liu, S. Ji, Y. Zhou, J. Wang, Euro. J. Inorg. Chem. 24 (2012) 3829;
(c) J. Liu, W. Liu, K. Chen, S. Ji, Y. Zhou, Y. Wan, D. Xue, P. Hodgson, Y. Li, Chem. Eur. J. 19 (2013) 9811;
(d) W. Liu, J. Liu, K. Chen, S. Ji, Y. Wan, Y. Zhou, D. Xue, P. Hodgson, Y. Li, Chem. Eur. J. 20 (2014) 824.
[3] Y. Zhu, J. Shi, W. Shen, X. Dong, J. Feng, M. Ruan, Y. Li, Angew. Chem. Int. Ed. 44 (2005) 5083.
[4] J.Y. Chen, B. Wiley, Z.Y. Li, D. Campbell, F. Saeki, H. Cang, L. Au, J. Lee, X.D. Li, Y.N. Xia, Adv. Mater. 17 (2005) 2255.
[5] U. Jeong, Y. Wang, M. Ibisate, Y.N. Xia, Adv. Funct. Mater. 15 (2005) 1907.
[6] L. Chen, Z. Song, X. Wang, S. Prikhodko, J. Hu, S. Kodambaka, R. Richards, Appl. Mater. Interf. 1 (2009) 1931.
[7] C. Chen, S. Abbas, A. Morey, S. Sithambaram, L. Xu, H. Garces, W. Hines, S. Suib, Adv. Mater. 20 (2008) 1205.
[8] N. Ren, B. Wang, Y. Yang, Y. Zhang, W. Yang, Y. Yue, Z. Gao, Y. Tang, Chem. Mater. 17 (2005) 2582.
[9] K. An, S. Kwon, M. Park, H. Na, S. Baik, J. Yu, D. Kim, J. Son, Y. Kim, I. Song, W. Moon, H. Park, T. Hyeon, Nano Lett. 8 (2008) 4252.
[10] N. Dhas, K.S. Suslick, J. Am. Chem. Soc. 127 (2005) 2368.
[11] J. Liu, D. Xue, Adv. Mater. 20 (2008) 2622.
[12] (a) Y.D. Yin, R.M. Rioux, C.K. Erdonmez, S. Hughes, G.A. Somorjai, A.P. Alivisatos, Science 304 (2004) 711;
(b) S. Peng, S. Sun, Angew. Chem. Int. Ed. 46 (2007) 4155.
[13] H.C. Zeng, Curr. Nanosci. 3 (2007) 177.
[14] G.L. Messing, S.C. Zhang, G.V. Jayanthi, J. Am. Ceram. Soc. 76 (1993) 2707.
[15] F. Caruso, R.A. Caruso, H. Mohwald, Science 282 (1998) 1111.
[16] J. Yuan, T. Zhou, H. Pu, J. Phys. Chem. Sol. 71 (2010) 1013.
[17] H. Shiho, N. Kawahashi, Colloid Polym. Sci. 278 (2000) 270.
[18] V. Salgueirino-Maceira, M. Spasova, M. Farle, Adv. Funct. Mater. 15 (2005) 1036.
[19] Q.R. Zhao, Y. Xie, T. Dong, Z.G. Zhang, J. Phys. Chem. C 111 (2007) 11598.
[20] X.X. Li, Y.J. Xiong, Z.Q. Li, Y. Xie, Inorg. Chem. 45 (2006) 3493.
[21] X. Wu, Y. Tian, Y. Cui, L. Wei, Q. Wang, Y. Chen, J. Phys. Chem. C 111 (2007) 9704.
[22] H.M. Abdelaal, M. Zawrah, B. Harbrecht, Chem. Eur. J. 20 (2014) 673.
[23] X. Sun, J. Liu, Y. Li, Chem. Eur. J. 12 (2006) 2039.
[24] M.M. Titirici, M. Antonietti, A. Thomas, Chem. Mater. 18 (2006) 3808.
[25] X.M. Sun, Y.D. Li, Angew. Chem., Int. Ed. 43 (2004) 597.
[26] H.M. Abdelaal, Chin. Chem. Lett. 25 (2014) 627.
[27] C. Yao, Y. Shin, L.Q. Wang, C.F. Windisch, W.D. Samuels, B.W. Arey, C. Wang, W.M. Risen, G.J. Exarhos, J. Phys. Chem. C 111 (2007) 15141.
[28] X'Pert Plus (1.0), Program for Crystallography and Rietveld analysis, Philips Analytical, Almelo (The Netherlands), 1999.
[29] M. Sevilla, A.B. Fuertes, Carbon 47 (2009) 2281.
[30] N. Baccile, G. Laurent, F. Babonneau, F. Fayon, M. Titirici, M. Antonietti, J. Phys. Chem. C 113 (2009) 9644.
[31] W.H. Suh, A. Jang, Y. Suh, K.S. Suslick, Adv. Mater. 18 (2006) 1832.
[32] H. Qian, G. Lin, Y. Zhang, P. Gunawan, R. Xu, Nanotech 18 (2007) 355602.
[33] H.P. Klug, L.E. Alexander, X-ray Diffraction procedures, Wiley, New York, 1959.
[34] T. Sakaki, M. Shibata, T. Miki, H. Hirosue, N. Hayashi, Bioresour. Technol. 58 (1996) 197.
[35] D. Ni, L. Wang, Y. Sun, Z. Guan, S. Yang, K. Zhou, Angew. Chem. Int. Ed. 49 (2010) 4223.
[36] I. Esparza, M. Paredes, R. Martinez, A. Couto, G. Sanchez, L. Velez, O. Dominguez, Mater. Sci. Appl. 2 (2011) 1584.
[37] K.S.W. Sing, D.H. Everett, R.A.W. Haul, L. Moscou, R.A. Pierotti, J. Rouquerol, T. Siemieniewska, Pure Appl. Chem. 57 (1985) 603.